Chemical Engineering Science 273 (2023) 118649

Contents lists available at ScienceDirect

Chemical Engineering Science

journal homepage: www.elsevier.com/locate/ces

Scale-up analysis of the oxidative dehydrogenation of ethane over $MoVTeNbO_x$ catalysts in an autothermal reactor

Jiakang Chen, Zhe Sun, Praveen Bollini *, Vemuri Balakotaiah *

William A. Brookshire Department of Chemical & Biomolecular Engineering, University of Houston, Houston, TX 77204, USA

HIGHLIGHTS

- Ignition-extinction analysis of autothermal ODHE reactor is presented.
- The operating windows of autothermal operation for ODHE are determined.
- The impact of pressure on ignition and extinction behaviors is analyzed.
- Autothermal and multi-tubular reactor designs for ODHE are compared.
- ODHE operated autothermally at high pressure is compared to ethane cracking.

GRAPHICAL ABSTRACT

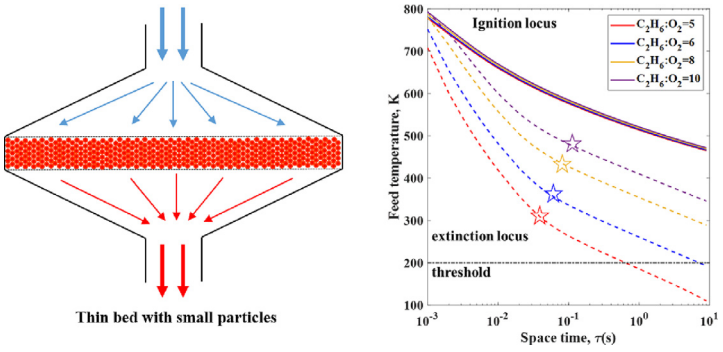

ARTICLE INFO

Article history:
Received 13 December 2022
Received in revised form 22 February 2023
Accepted 14 March 2023
Available online 17 March 2023

Keywords:
Oxidative dehydrogenation
Finite heat dispersion model
Ignition and extinction
Autothermal reactor
Pressure effects

ABSTRACT

We examine the oxidative dehydrogenation of ethane (ODHE) using a one-dimensional finite heat dispersion model and present a comprehensive ignition-extinction analysis of the process in an adiabatic autothermal reactor. The six-step kinetic model used in the scale-up studies was derived from lab-scale reactor data and validated over a wide range of experimental conditions. We investigate the impact of ethane to oxygen feed ratio, space time, and bed length on the region of autothermal operation as a function of feed temperature. The results reveal that ethane conversion and ethylene selectivity are not monotonic at the extinction point and there exists an optimum set of design and operating conditions. We also report the impact of operating pressure in terms of fixed linear and mass velocities. Our analysis and comparisons show that ODHE, when operated at high pressure, may lead to performance that is comparable to the ethane steam cracking process.

1. Introduction

The discovery and rapid development of shale gas in the past 20 years has reduced the price of natural gas, thereby promoting its use as feedstock to produce a variety of bulk chemicals (Bilgen and Sarıkaya, 2016). As an important building block of the petrochemical industry, ethylene is used to produce a variety of chemical intermediates and polymers (Cavani et al., 2007). Currently, steam cracking of ethane, naphtha or other hydrocarbons is the predominant route for producing ethylene (Amghizar et al., 2017; Ren et al., 2006). In fact, this highly endothermic reaction is considered one of the most energy intensive processes in the chemical industry because of the high operating temperature and the difficulty of purification and separation steps (Abdelbaki et al., 2021; Qian et al., 2022). The cumulative CO_2 emissions from steam cracking of ethane amount to about 1.0 kg CO_2 per kg of ethylene produced (Ren et al., 2006). Among alternative technologies, oxidative dehydrogenation of ethane is one of the most promising routes to produce ethylene with lower energy consump-

* Corresponding authors.
E-mail addresses: ppbollini@uh.edu (P. Bollini), bala@uh.edu (V. Balakotaiah).

https://doi.org/10.1016/j.ces.2023.118649
0009-2509/

Nomenclature

Roman letters:

a_v	heat (mass) transfer area per unit bed volume, m^{-1}
C_{pv}	volumetric heat capacity of the reaction mixture, J/(m^3*K)
d_p	catalyst particle size, m
$D_{m,j}$	mass diffusivity of species j, m^2/s
$D_{eff,j}$	effective mass diffusion coefficient of species j, m^2/s
h	heat transfer coefficient, J/(s*m^2*K)
ΔH_j^{st}	reaction enthalpy at standard condition for reaction j, kJ/mol
$\Delta H_{r,i}$	reaction enthalpy for reaction i, kJ/mol
k_c	mass transfer coefficient, m/s
L	length scale of the reactor bed, m
$Pe_{eff,m,j}$	effective mass Peclet number of species j
$Pe_{eff,h}$	effective heat Peclet number
r_i	reaction rate i, s^{-1}
T	reaction temperature,*K*
T^{in}	inlet reaction temperature,*K*
ΔT_{ad}	adiabatic temperature rise, K
$< u >$	averaged gas velocity, m/s
y_j	mole fraction of species j
y_j^{in}	inlet mole fraction of species j
z	dimensionless position along the reactor bed

Greek letters:

$\alpha_{s,eff}$	catalyst thermal diffusivity, m^2/s
α_{eff}	effective thermal dispersion coefficient, m^2/s
ν_{ij}	stoichiometric coefficient of spiecies j for reaction i
τ_{mi}	characteristic inter-phase mass transfer time, s
τ_{hi}	characteristic inter-phase heat transfer time, s
τ	space time,*s*
$\tau_{M,j}$	mass dispersion time of species j,*s*
τ_H	heat dispersion time,*s*
$< \rho C_{pv}(T) >$	averaged molar heat capacity of the reaction mixture, J/(mol*K)

tion and greenhouse gas emissions. It is reported that the ODHE process could provide about 20–30% energy savings (Gaffney et al., 2021b; Luongo et al., 2021) and about 82% reduction in CO_2 emissions (Haribal et al., 2017) compared with steam cracking. However, there are two major challenges to the commercialization of the ODHE process. The first is the design and synthesis of an active, selective, and stable catalyst. The second is the design of a reactor to remove the generated heat efficiently from this highly exothermic reaction system.

In recent years, it was found that multi-metallic mixed oxides containing Mo, V, Te and Nb show remarkable selectivity for the ODHE reaction (Botella et al., 2004; Che-Galicia et al., 2014; Gaffney et al., 2021a; Melzer et al., 2019; Nguyen et al., 2012). This was followed by an intensive focus in the literature on improving catalyst performance through modifying catalyst structure and various post-treatments (Chu et al., 2015; Kolen'ko et al., 2011; Sanfiz et al., 2010). It is reported that MoVTeNbOx catalyst is able to convert ethane to ethylene with about 60% conversion and 90% selectivity at around 400 °C, thereby reaching the industrial goal (Gaffney and Mason, 2017). Annamalai et al. (Annamalai et al., 2018) have reported the kinetics of the oxidative dehydrogenation reaction over a $MoVTeNbO_x$ catalyst. Lemonidou's group (Heracleous and Lemonidou, 2006a, 2006b) used transient experiments with isotopic $^{18}O_2$ to derive a kinetic model over Ni-Nb-O catalysts. Che-Galicia et al. (Che-Galicia et al., 2014) have reported a pseudo-global kinetic model validated by their experimental results over $MoVTeNbO_x$ at sub-ambient reactant pressures. Recently, Chen et al. proposed a two-site global kinetic model based on the M1 phase catalyst that describes ODHE performance over a range of reaction temperatures and reactant/product pressures (Chen et al., 2022). In this study, we use this experimentally validated model to investigate the ignition-extinction features of the ODHE process.

Tubular packed bed reactors are widely used to carry out many exothermic reactions such as ethylene epoxidation (Nawaz, 2016) and ammonia synthesis (Ghani and Iranshahi, 2019). A typical multi-tubular reactor contains thousands of small tubes (as small as 2.54 cm in diameter) with a high ratio of the heat transfer area to reaction volume. Circulating coolant is used to remove a large amount of reaction heat through the reactor shell and to maintain the reactor close to isothermal conditions. However, it is possible to remove the heat for strongly exothermic reactions such as ODHE operating at high pressure over highly active catalyst only by diluting the reactants/catalyst or using large space times (Chen et al., 2021). Rodríguez et al. (Rodríguez et al., 2011) coated Ni-Nb-O catalyst over raschig-rings inside the tubes and used a 4 m long bed to avoid hot spots in the multi-tubular reactor and multi-tubular membrane reactor. Che-Galicia et al. (Che-Galicia et al., 2015) reported that the ODHE system could be implemented in the multi-tubular reactor with low active catalyst density (75 kg/m^3) and about 50% to 90% reactant dilution over $MoVTeNbO_x$ catalysts. Fazlinezhad et al. (Fazlinezhad et al., 2019) designed a reactor with 10,000 reactor tubes and 40% nitrogen dilution to remove the heat generated at 5 bar. However, autothermal reactor or autothermal operation (AO) can address heat transfer concerns and achieve high ethylene yield. Autothermal operation is the intentional operation near the extinction point on the ignited branch where the reactor is close to adiabatic conditions. In AO, there is no heat addition to the reactor and no intentional heat removal through the wall except for some minor heat loss to the surroundings (Balakotaiah et al., 2021). The reaction heat is mainly removed by the convection of the cold reactants. Balakotaiah et al. (Balakotaiah et al., 2019) discussed several advantages of autothermal operation: compact reactor with low feed temperature, low pressure drop and high productivity. Multiple steady-states normally exist in reactors with strong thermal-backmixing and exothermic reactions. Sarsani et al. (Sarsani et al., 2017) recently demonstrated the ignition and extinction behaviors of the OCM reaction using experiments and proved that it is possible to carry out oxidative coupling of methane in autothermal reactors. Sun et al. (Sun et al., 2020) performed a bifurcation analysis of the OCM reactor and showed that a scaled-up autothermal reactor can reach 20% methane conversion and 80% C_2 selectivity. However, there have not been studies on autothermal reactor design that can be plausibly implemented for the ODHE process. In this work, we show that ODHE can be operated autothermally at elevated pressure with ambient temperature feeds and without external heat input.

The main goal of this work is to provide a comprehensive bifurcation analysis of oxidative dehydrogenation of ethane using a global kinetic model developed from recent experimental results over the $MoVTeNbO_x$ catalyst. In the next section, we review the reaction network and kinetic model over the MoVTeNbOx catalyst. Moreover, we present and use a 1D pseudo-homogeneous finite heat dispersion model for our ignition-extinction analysis. In section 3, we start with three limiting reactor models: long bed or

plug flow reactor (PFR), short bed or continuous stirred-tank reactor (CSTR) and lumped thermal reactor (LTR). The impacts of design and reaction conditions including ethane/oxygen feed ratio, space time and bed length on the ignition and extinction locus are then discussed. The optimum operating window where ethane conversion and ethylene selectivity are maximized is also determined. In section 4, we demonstrate the impact of operating pressure on the ODHE process for two cases: fixed linear velocity and fixed mass velocity. Increasing operating pressure with fixed mass velocity leads to larger operating windows with high conversion and selectivity but with significantly lower productivity. Further, we model and compare multi-tubular and autothermal reactor designs using the full kinetic model and conclude that an autothermal reactor operated at higher pressure has a much higher productivity than the multi-tubular reactor. Finally, we show that autothermal operation of ODHE at high pressure can deliver similar or better performance compared to the ethane cracking process. In the last section, we summarize our results and discuss some limitations and possible extensions of this work.

2. Model development

2.1. Global kinetic model of ODHE

The reaction scheme of the ODHE process over the $MoVTeNbO_x$ catalyst is taken from experimental results discussed in an earlier publication (Chen et al., 2022). The reaction scheme consists of 4 parts: ethane can be converted to ethylene through primary dehydrogenation reaction (step 1); CO_x can be produced from deep oxidation of ethane (steps 2 and 3); CO_x can also be generated from secondary oxidation of ethylene (steps 4 and 5); CO can be further oxidized into CO_2 through step 6.

Step 1	$C_2H_6 + 0.5O_2 \rightarrow C_2H_4 + H_2O$, $\Delta H_1^0 = -105kJ/mol$	(1)
Step 2	$C_2H_6 + 2.5O_2 \rightarrow 2CO + 3H_2O$, $\Delta H_2^0 = -863kJ/mol$	(2)
Step 3	$C_2H_6 + 3.5O_2 \rightarrow 2CO_2 + 3H_2O$, $\Delta H_3^0 = -1428kJ/mol$	(3)
Step 4	$C_2H_4 + 2O_2 \rightarrow 2CO + 2H_2O$, $\Delta H_4^0 = -757kJ/mol$	(4)
Step 5	$C_2H_4 + 3O_2 \rightarrow 2CO_2 + 2H_2O$, $\Delta H_5^0 = -1323kJ/mol$	(5)
Step 6	$CO + 0.5O_2 \rightarrow CO_2$, $\Delta H_6^0 = -283kJ/mol$	(6)

All 6 oxidation reactions are highly exothermic. Table 1 shows the adiabatic temperature rise of each step calculated at specific reaction conditions. For example, the adiabatic temperature rise for the deep oxidation of ethane (step 2 and step 3) is about 500–900 K, which is much higher than that for the primary dehydrogenation reaction (step 1). [Remark: Rows 4 and 5 of the Table 1 give the ΔT_{ad} for a hypothetical case in which feed contains only C_2H_4 and O_2. When the feed contains no C_2H_4, the temperature rise due to secondary oxidation is smaller]. Inclusion of these highly exothermic side reactions could render multi-tubular reactors more difficult to control within a narrow temperature range while maintaining desired selectivity. The equations that describe the rate expressions of the ODHE process are listed in Section S1 of the Supplementary Information. Kinetic parameters used including the pre-exponential factor and activation energies are listed in **Table S2**. These rate expressions and kinetic parameters present two key features from the standpoint of reactor design. The oxygen order of the primary dehydrogenation reaction (step 1) can vary from 0 to 1 depending on the oxygen partial pressure, as shown in **Table S1**. More specifically, oxygen order of the primary dehydrogenation reaction increases from 0 to 1 while oxygen order of all other reaction steps remains unchanged at 0.5 as oxygen partial pressure decreases. The differences in oxygen order indicate that ethylene selectivity can be optimized by adjusting the oxygen mole fraction present in the feed. Another observation is that the activation energy of the dehydrogenation reaction (step 1) is only 89.4 kJ/mol, 30–40 kJ/mol lower than the activation energy of side reactions, as shown in **Table S2**. The lower activation energy of the desired dehydrogenation reaction indicates that rates of total oxidation side reactions increase significantly faster than the desired dehydrogenation rate. Lower reaction temperatures should therefore favor higher ethylene selectivities. Both Valente et al. (Valente et al., 2014) and Rahman et al. (Rahman et al., 2010) have previously observed that ethylene selectivity decreases with increasing reaction temperature. These two kinetic features enable us to maximize ethane conversion and ethylene selectivity by tuning the ethane to oxygen ratio, space time, and bed length.

2.2. Reactor model

The characteristic inter-phase mass and heat transfer times are calculated as follows:

$$\tau_{mi} = \frac{1}{k_c a_v}, \tag{7}$$

$$\tau_{hi} = \frac{C_{pv}}{h a_v}, \tag{8}$$

where k_c is the gas to solid mass transfer coefficient, C_{pv} is the volumetric heat capacity of the reaction mixture, h is the heat transfer coefficient and a_v is the heat (mass) transfer area per unit bed volume. **Table S3** lists typical inter-phase mass and heat transfer times for different catalyst particle sizes and reaction temperatures. It is found that the inter-phase mass transfer time increases from 2 ms to 65 ms when particle size increases from 1 mm to 8 mm at 650 K. As temperature increases from 650 K to 750 K, the mass transfer time decreases from 65 ms to 56 ms for the 8 mm catalyst particle. Generally, inter-phase heat and mass transfer times are in the range of 1–5 ms for the 1 mm catalyst particle - two to three orders of magnitude smaller than the typical space times reported in the literature for autothermal operation (0.1–1 s) (Che-Galicia

Table 1
ODHE adiabatic temperature rise for each step with different $C_2H_6/C_2H_4 : O_2$ feed ratios, T_f=310 K, P_{total}=1 bar.

	ΔT_{ad}(K)			
Feed ratios C_2H_6/C_2H_4:O_2	4:1	6:1	8:1	10:1
Reaction steps				
1	541	398	323	271
2	799	585	481	407
3	895	665	548	454
4	1021	770	632	533
5	1099	863	707	599

et al., 2014; López Nieto et al., 2002). The much smaller heat and mass transfer time scales compared to space time suggest that we can neglect heat and mass transfer limitations for catalyst particles of size below 1 mm. Additionally, we can assume small variations in physical properties and dispersion coefficients and simply apply their average values in the pseudo-homogeneous model that is sufficient for analyzing ignition and extinction behavior in autothermal operation. The steady-state species and energy balances for the adiabatic case are given by:

$$\frac{\tau}{\tau_{M,j}}\frac{d^2y_j}{dz^2}-\frac{dy_j}{dz}+\tau\sum_{i=1}^{N}\upsilon_{ij}r_i\left(\bar{y},T\right)=0,j=1,2,\cdots N, \tag{9}$$

$$\frac{\tau}{\tau_H}\frac{d^2T}{dz^2}-\frac{dT}{dz}+\tau\sum_{i=1}^{N}\frac{\left(-\Delta H_{r,i}(T)\right)r_i\left(\bar{y},T\right)}{<\rho C_{pv}(T)>}=0, \tag{10}$$

with the boundary conditions:

$$\frac{\tau}{\tau_M}\frac{dy_j}{dz}=y_j-y_j^{in},at\ z=0, \tag{11}$$

$$\frac{dy_j}{dz}=0,at\ z=1, \tag{12}$$

$$\frac{\tau}{\tau_H}\frac{dT}{dz}=T-T^{in},at\ z=0, \tag{13}$$

$$\frac{dT}{dz}=0,at\ z=1, \tag{14}$$

where τ is the space time, y_j is the mole fraction of species j, z is the dimensionless position along the reactor bed, υ_{ij} is the stoichiometric coefficient of species j in reaction i, $r_i\left(\bar{y},T\right)$ is the rate of reaction i having unit of s^{-1}, $-\Delta H_{r,i}(T)$ is the reaction enthalpy at a specific temperature T, $<\rho C_{pv}(T)>$ is the average heat capacity of the reaction mixture, and $\tau_{M,j}$ and τ_H are the mass dispersion time of species j and heat dispersion time, respectively. Mass and heat dispersion times are calculated using the following equations:

$$\tau_{M,j}=\frac{L^2}{D_{eff,j}},j=1,2,\cdots N, \tag{15}$$

$$\tau_H=\frac{L^2}{\alpha_{eff}}, \tag{16}$$

where L is the length scale of the reactor bed, $D_{eff,j}$ is the effective mass dispersion coefficient of species j that depends on species molecular diffusivity (calculated by the Fuller equation (Fuller, 1965)) as well as bed properties and α_{eff} is the effective thermal dispersion coefficient of the catalyst bed. Detailed calculations of $D_{eff,j}$ and α_{eff} values can be found in Sun et al. (Sun et al., 2019). Steady-state bifurcation diagrams of this finite heat dispersion model are computed numerically using the pseudo arc-length continuation method through Python and Matlab. It should be noted that the pseudo-homogeneous model analyzed here is valid only for small particle sizes ($\leq$ 1 mm) and space time exceeding about 50 ms for which both inter and intra-particle gradients can be neglected for the specific ODHE kinetics considered here.

3. Steady-state bifurcation analysis

3.1. Ignition and extinction behaviors

Before discussing the finite heat dispersion model, we analyze the ignition and extinction behavior of three limiting reactor models: the long bed or plug flow reactor (PFR) model, the thin bed or continuous stirred-tank reactor (CSTR) model, and the lumped thermal reactor (LTR) model. If the heat and mass dispersion times are much smaller than the space time (which can be realized in a very thin catalyst bed), the finite heat dispersion model can be simplified to the ideal CSTR model. The ideal PFR model can be reached when the heat and mass dispersion times are much larger than the space time, and this limit can be approached in a very long bed. However, if the mass dispersion time is much larger than the space time while the heat dispersion time is much smaller than the space time, the finite heat dispersion model approaches the LTR model which corresponds to perfect thermal backmixing but zero species backmixing. Strong thermal backmixing akin to the LTR model can be achieved either by using catalyst particles having a high thermal conductivity or by coating the catalyst powder on a high conductivity support such as a metallic monolith. Fig. 1 compares the bifurcation diagrams of exit temperature, exit ethane and oxygen conversion, and exit ethylene selectivity as a function of feed temperature at a fixed space time of 0.2 s and a fixed $C_2H_6:O_2$ ratio of 6 for these three limiting models. From these bifurcation results, we observe that whereas CSTR and LTR models show a large region of multiplicity, the PFR displays no region of multiplicity. These results show that temperature and conversion increase or decrease rapidly at the critical feed temperature corresponding to the ignition and extinction points. Comparing the PFR and LTR curves, it can be observed that thermal backmixing affects both the ignition as well as the extinction point. Comparison of the LTR and CSTR curves, on the other hand, indicates that species backmixing shrinks the region of multiplicity, due to the fact that backmixing lowers average reactant concentrations. For the ODHE kinetics of relevance to our calculations, lower reactant concentrations generally mean lower reaction rates and hence a smaller region of multiplicity. Fig. 1**b and 1d** show that the LTR model leads to higher ethane conversions and ethylene selectivity at the extinction point compared to the CSTR model. As discussed in the previous section, extremely low oxygen mole fractions (<1%) steer selectivity to CO_x because the rates of the dehydrogenation reaction approach first order behavior in oxygen, unlike the rates of side reactions that remain half order in oxygen regardless of oxygen pressure. The LTR model tends to have an oxygen mole fraction gradient along the reactor bed due to lack of mass dispersion rather than maintaining extremely low oxygen mole fraction (<1%) as in CSTR model. Therefore, LTR model has higher ethane conversion and ethylene selectivity than CSTR model. Another reason for the LTR model exhibiting better performance is that negligible species dispersion lowers both the feed temperature as well as the extinction temperature compared with the CSTR model. The lower operating temperature for the LTR translates to better catalytic performance because the activation energy of the desired dehydrogenation reaction is significantly lower than those of side reactions. Generally speaking, the optimal operating point for autothermal operation falls on the ignited branch close to the extinction point. We note that at this point we can simultaneously obtain almost complete conversion of the limiting reactant (O_2) as well as high ethylene selectivity by feeding the reaction mixture at ambient temperature. Based on these considerations, the LTR model has the largest region of multiplicity and the best catalytic performance near the extinction point among the three ideal reactor models tested. These ideal reactor models, however, only provide limiting behavior that is challenging to replicate in practice, and hence require us to use more realistic models such as the finite heat dispersion model to more accurately investigate ignition and extinction behavior, as discussed next.

Generally speaking, the optimum operating point is about 5–10 K higher than the extinction point on the ignited branch where oxygen is nearly completely converted. In autothermal operation, the optimum point of operation can be reached using

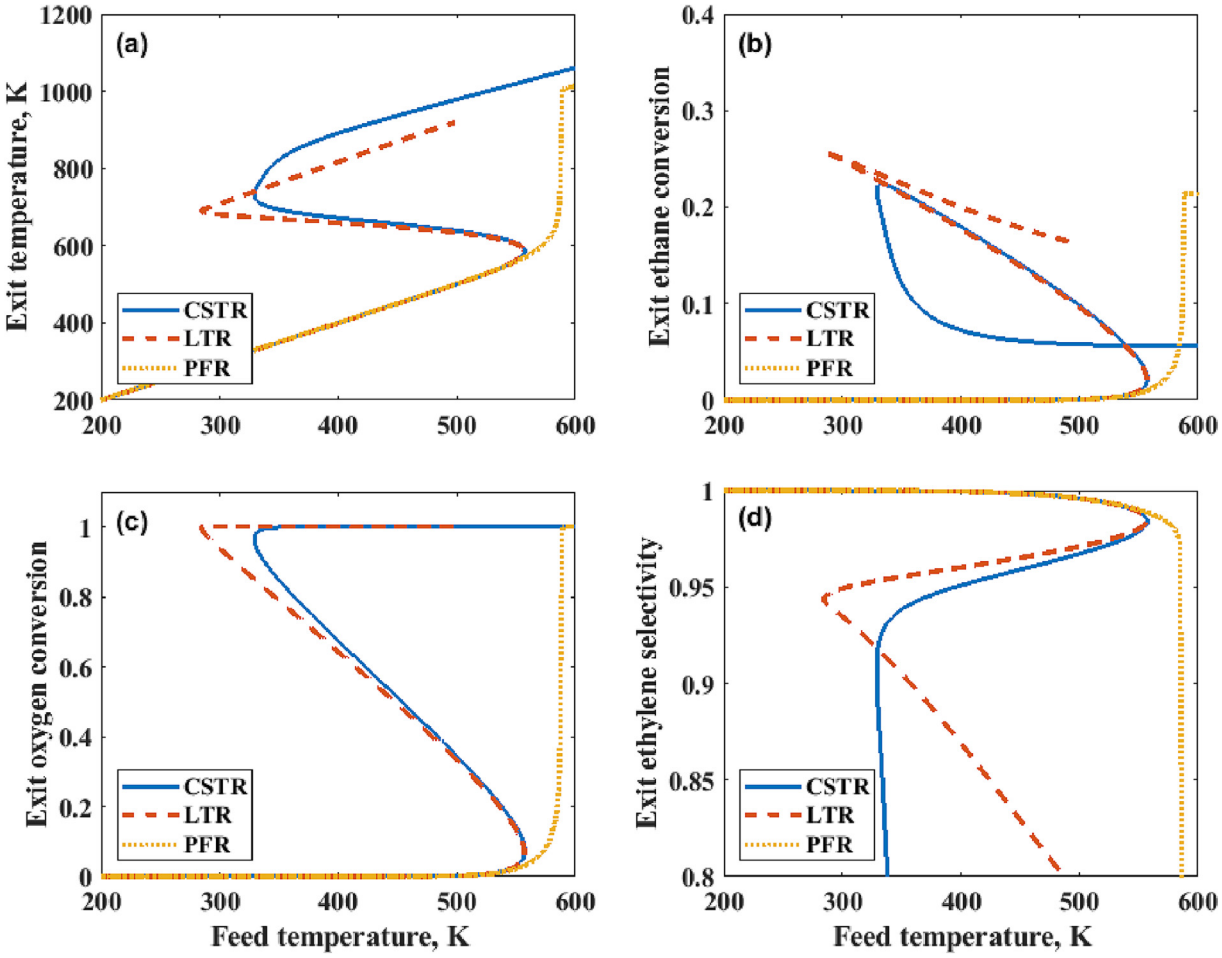

Fig. 1. Computed bifurcation diagrams of exit (a) temperature, (b) ethane conversion, (c) oxygen conversion, and (d) ethylene selectivity versus feed temperature for long bed (PFR), thin bed (CSTR), and LTR models. Reaction conditions: $C_2H_6 : O_2$=6, τ=0.2 s.

proper start-up procedures: the catalyst bed is initially heated to reach the ignited branch and catalyst deactivation is avoided; feed conditions are carefully adjusted to avoid overheating or quenching of the catalyst bed (Balakotaiah et al., 2019). Fig. 2 shows ignition and extinction loci in the plane of feed temperature and space time for different $C_2H_6 : O_2$ ratios calculated using the finite heat dispersion model (for a bed length L = 4 mm). The adiabatic temperature rise increases with decreasing $C_2H_6 : O_2$ ratio as shown in the Table 1. It is found that the space time at the ignition point is very high when the feed temperature is close to ambient temperature, indicating that proper start-up procedure is required to reach the ignited branch. The region of multiplicity increases with increasing space time or decreasing feed temperature for a fixed feed ratio (adiabatic temperature rise). The results show that extinction loci are more sensitive to the feed ratio than ignition loci. Balakotaiah et al. (Balakotaiah et al., 2021) have pointed out that the space time at the extinction point can vary exponentially with adiabatic temperature rise (feed ratio), while the ignition point is roughly inversely proportional to the same. These trends in which extinction loci change significantly with feed ratio, unlike ignition loci that are insensitive to feed ratio, result in a region of multiplicity that expands as the feed ratio decreases. We focus only on the extinction locus in the later discussion rather than the ignition locus because the optimum operating point relates to the extinction point. Several important conclusions can be drawn from these calculations. The ethane boiling temperature is approximately 184 K, and therefore the feed temperature should be at least that value. Moreover, the $MoVTeNbO_x$ catalyst is susceptible to deactivation above 773 K, implying that the operating temperature must be maintained below this limit. For example, the adiabatic temperature rise value for a feed ratio of 6 lies between 398 and 450 K depending on the product selectivity (typical ethylene selectivities are greater than 90%). The upper bound on the feed temperature will be about 350 K, indicated by the blue star in Fig. 2. In terms of space time, the operating window at a feed ratio of 6 lies between 0.06 and 8 s, larger than that at a ratio of 5, which ranges between 0.04 and 0.6 s. Although a lower feed ratio leads to a smaller operating window, exit ethane conversions are always higher. The autothermal reactor yield of this ODHE process can be optimized using an ignition and extinction analysis by tuning the space time, feed ratio, and feed temperature.

3.2. Impact of C_2H_6:O_2 feed ratio

The pseudo homogeneous finite heat dispersion model has several important parameters: space time, heat and mass dispersion time (or bed length and thermal conductivity), C_2H_6/O_2 feed ratio (adiabatic temperature rise), and feed temperature. We first discuss the impact of the C_2H_6:O_2 feed ratio on ignition and extinction behavior. As mentioned earlier, a lower feed ratio means higher per pass conversion but also higher adiabatic temperature rise values and a larger region of multiplicity. Fig. 3 illustrates the impact of feed ratio on exit temperature, ethane and oxygen conversion, and ethylene selectivity at a fixed space time of 0.2 s and a bed

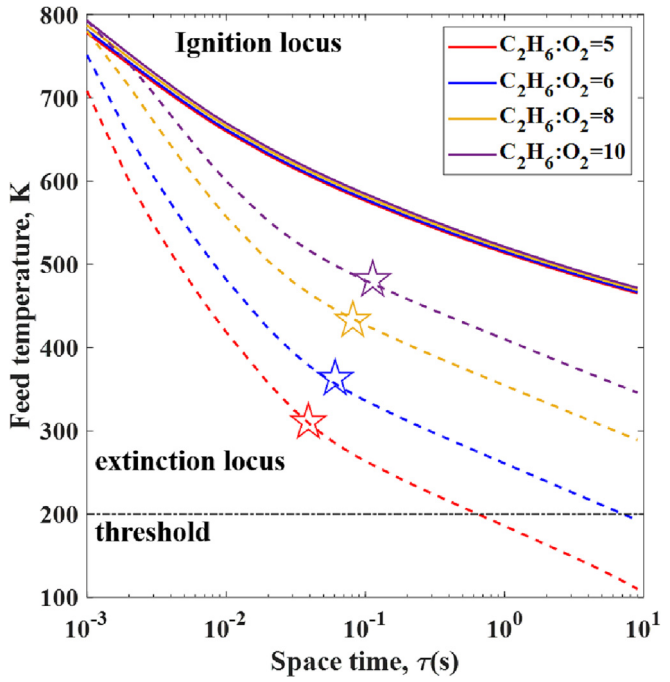

Fig. 2. Computed ignition and extinction loci for the finite heat dispersion model in the plane of feed temperature and space time, the star symbols represent the upper limit of feed temperature and the dash-dotted line represents the lower limit of feed temperature. Calculations were carried out for a bed length of 4 mm.

length of 4 mm. With decreasing feed ratios, the ignition point remains almost unchanged while the extinction point moves to much lower feed temperatures, leading to a larger region of multiplicity. Although the feed temperature at the extinction point is reduced, the exit temperature still increases with decreasing feed ratio due to higher adiabatic temperature rise values. It is also found that as the feed ratio increases, the ethylene selectivity near the extinction point increases while the ethane conversion decreases, as shown in Fig. 3**b and 3d**. The activation energy of the desired dehydrogenation reaction is lower than that of side reactions, and therefore lower exit temperatures favor the desired dehydrogenation reaction, implying that higher feed ratios (i.e. lower exit temperatures) can yield higher ethylene selectivity. As for ethane conversion, lower feed ratios lead to higher per pass ethane conversion.

Fig. 3**b** shows that ethane conversion reaches its maximum value at the extinction point and keeps decreasing on the ignited branch as feed temperature increases. For the specific ODHE kinetics under consideration, side reactions are favored at higher temperature and extremely low oxygen concentrations, as discussed in the Section 2. Side reactions become dominant on the ignited branch after the extinction point, where oxygen concentrations are very low and exit temperatures are high. Since side reactions consume more moles of oxygen per mole of hydrocarbon than the dehydrogenation reaction (equations 1–6) and oxygen is the limiting reactant, the ethane conversion decreases after passing the extinction point and finally reaches an asymptotic value (about 0.05). These decreases in ethane conversion are a direct consequence of the predominance of oxygen-intensive deep oxidation reactions on the ignited branch.

3.3. Impact of space time

The impact of space time on exit temperature, ethane and oxygen conversion, and ethylene selectivity at a constant C_2H_6:O_2 feed ratio of 6 and constant bed length of 4 mm is illustrated in Fig. 4. With space time increasing from 0.1 to 0.8 s, both ignition and extinction points move to lower feed temperature. Since extinction points are more sensitive to space time than ignition points, the region of hysteresis still expands as space time increases. Large space times strengthen thermal backmixing and favor larger regions of multiplicity. It can be observed that exit temperatures at the extinction point are lower at higher space times due to lower feed temperatures. Oxygen is almost fully converted at the extinction point as shown in the Fig. 4**c**. Lower exit temperatures favor the desired dehydrogenation reaction which consumes more ethane per mole of oxygen compared to side reactions. Higher space times therefore yield more favorable ethane conversion and ethylene selectivity near the extinction point on the ignited branch.

It is found, however, that the exit temperature on the ignited branch for the same feed temperature is higher at larger space times. Larger space times favor species back-mixing, and hence oxygen concentrations on the ignited branch are lower, thereby favoring side reactions to the desired dehydrogenation reaction. As a result, side reactions become more dominant on the ignited branch and generate more heat at higher space times.

We would like to point out that it is feasible to achieve 23% ethane conversion and 92% selectivity with a C_2H_6:O_2 feed ratio of 6 and a space time of 0.2 s by feeding the reaction mixture at 310 K for this ODHE process. A feed ratio of 6 may be preferred because it leads to a reasonable feed temperature and a low operating temperature on the ignited branch [Remark: A feed ratio of 6 is also outside of the upper flammability limit]. Feed ratios below 6 yield higher ethane conversion but bring the extinction feed temperature below ambient temperature and also lead to a lower ethylene selectivity. Feed ratios greater than 6 result in higher ethylene selectivity but lower per pass ethane conversion. A high space time such as 0.8 s decreases the feed temperature at extinction to about 270 K and achieves close to 95% ethylene selectivity and 25% ethane conversion, but also decreases the productivity.

3.4. Impact of bed length

Mass and heat Peclet numbers represent the extent of heat and mass dispersion within the catalyst bed, and are calculated using the following equations:

$$Pe_{eff,m,j} = \frac{L < u >}{D_{eff,j}} = \frac{L^2}{\tau D_{eff,j}}, j = 1, 2, \cdots N, \tag{17}$$

$$Pe_{eff,h} = \frac{L < u >}{\alpha_{eff}} = \frac{L^2}{\tau \alpha_{eff}}. \tag{18}$$

From these equations, heat and mass Peclet numbers could increase by a factor of 16 as bed length increases by a factor of 4 at a fixed space time. For a fixed space time, decreasing the bed length could decrease heat and mass Peclet numbers, and therefore approach the thin bed limit of the ideal CSTR model. On the other hand, having a longer catalyst bed implies higher heat and mass Peclet numbers, leading to significant axial temperature and concentration gradients. Fig. 5 shows the computed bifurcation diagrams for four different reactor lengths at a fixed C_2H_6 and O_2 feed ratio of 6 and space time of 0.2 s. As the bed length increases from 2 mm to 15 mm, the heat Peclet number increases from 0.02 to 1.1 while the mass Peclet number varies from 2 to 112, resulting in weaker mass and heat dispersion. Bed length has a minor impact on the ignition point but moves the extinction point to higher feed temperatures, and therefore shrinks the region of multiplicity. It can also be seen that the maximum ethane conversion and ethylene selectivity are obtained at the extinction point and for the

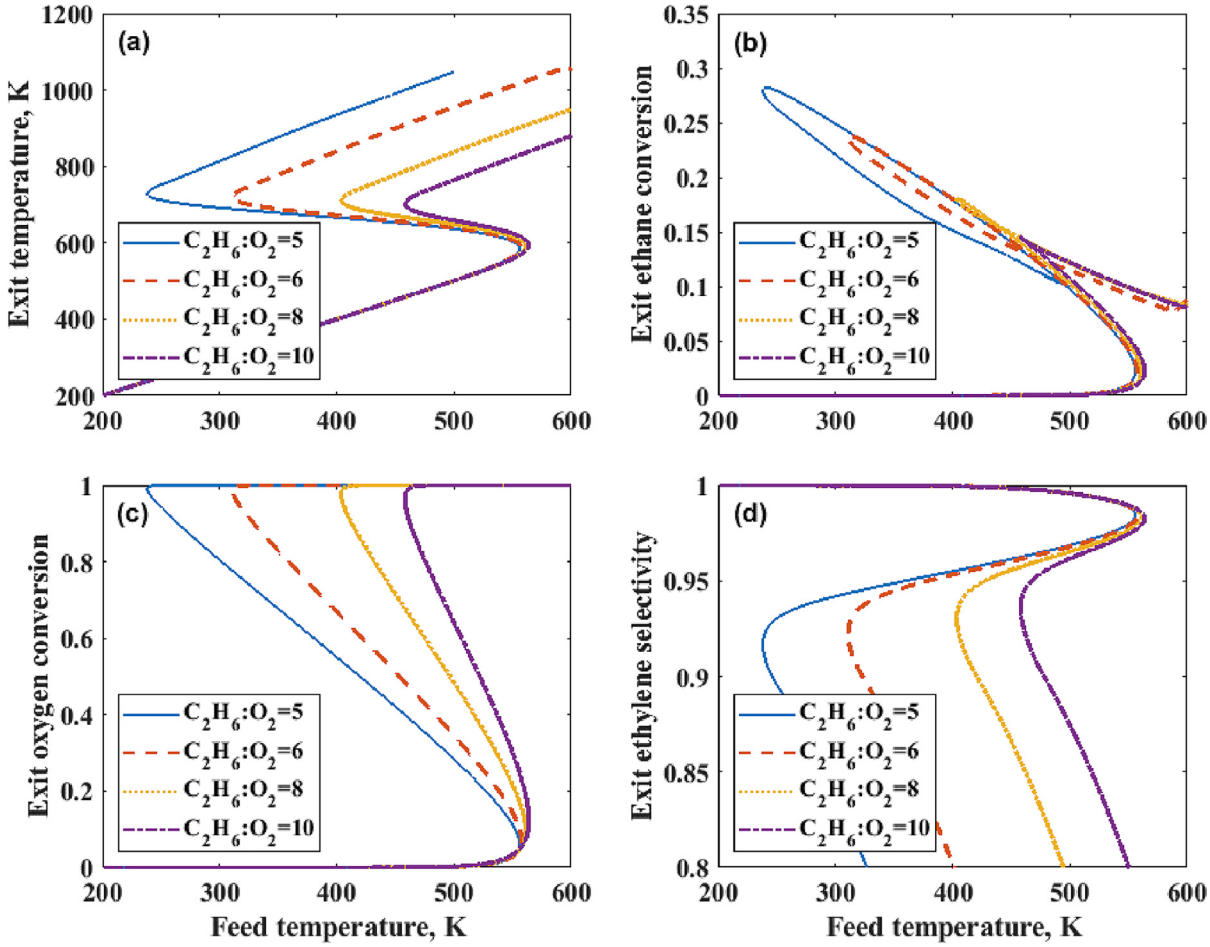

Fig. 3. Computed bifurcation diagrams of exit (a) temperature, (b) ethane conversion, (c) oxygen conversion, and (d) ethylene selectivity versus feed temperature with different feed ratios for the finite heat dispersion model. Reaction conditions: τ=0.2 s, bed length is 4 mm.

intermediate bed length (of 8 mm) as shown in Fig. 5**b and 5d**. This is due to the relative difference in oxygen order and activation energy between desired dehydrogenation and side reactions. As discussed in section 2, the oxygen order of the main dehydrogenation reaction shifts from close to zero order to first order as the oxygen mole fraction decreases. According to our calculations, keeping the mole fraction of oxygen between 1% and 10% will facilitate the desired dehydrogenation reaction. On the other hand, side reactions would be favored when oxygen mole fractions fall below 1%. Since the activation energy of the required dehydrogenation reaction is lower than those of side reactions, lower exit temperatures would tend to make the dehydrogenation reaction more predominant. It can therefore be concluded that a bed with a lower exit temperature and oxygen mole fraction (but higher than 1%) tends to provide the highest ethane conversion and ethylene selectivity. Fig. 6 illustrates the temperature, oxygen mole fraction, and ethylene selectivity profiles at the extinction point along the catalyst bed with a constant C_2H_6:O_2 feed ratio of 6 and space time of 0.2 s. Comparing the curves for the 2 and 8 mm beds, the 2 mm bed has very low oxygen mole fraction (below 1%) and higher exit temperature along the catalyst bed, which explains the lower ethylene selectivity as shown in Fig. 6**c**. Comparing the curves for the 8 and 15 mm beds, the 15 mm bed has a higher exit temperature at the end of the reactor where side reactions rates are much higher, resulting in a lower ethylene selectivity. We therefore observe that the ethane conversion and ethylene selectivity decrease from 25% to 22% and from 94% to 93%, respectively, as the bed length increases from 8 to 15 mm. These results clearly demonstrate how, for the specific ODHE kinetics under consideration, we can achieve maximum catalytic performance by tuning oxygen concentration and catalyst temperature by varying reactor bed length.

4. Analysis of pressure effects

Many catalytic partial oxidation reactions such as the oxidative coupling of methane (OCM) and ethylene oxide production are carried out at elevated pressure due to economic considerations. Chen et al. (Chen et al., 2020) pointed out that the optimum pressure range for OCM is between 5 and 10 bar in an autothermal reactor. Commercial ethylene oxide production is implemented in 10–15 m long multi-tubular reactors over a silver-based catalyst at a pressure of 10–20 bar (Matar and Hatch, 2001). In these reactors, there is also a need to control per pass conversion to less than 10% and to use several thousand tubes so that the generated heat can be removed efficiently for these exothermic reactions at higher pressures. Autothermal operation, on the other hand, allows us to circumvent this limitation because adiabatic temperature rise is independent of pressure to a first approximation and all of the heat generated can be removed through convection of cold feeds at high operating pressures. Typically, we can either vary the linear velocity or the mass velocity to change the space time when operating at high pressures. Productivity is an important factor in the scale-up of the process and is proportional to total pressure and inversely

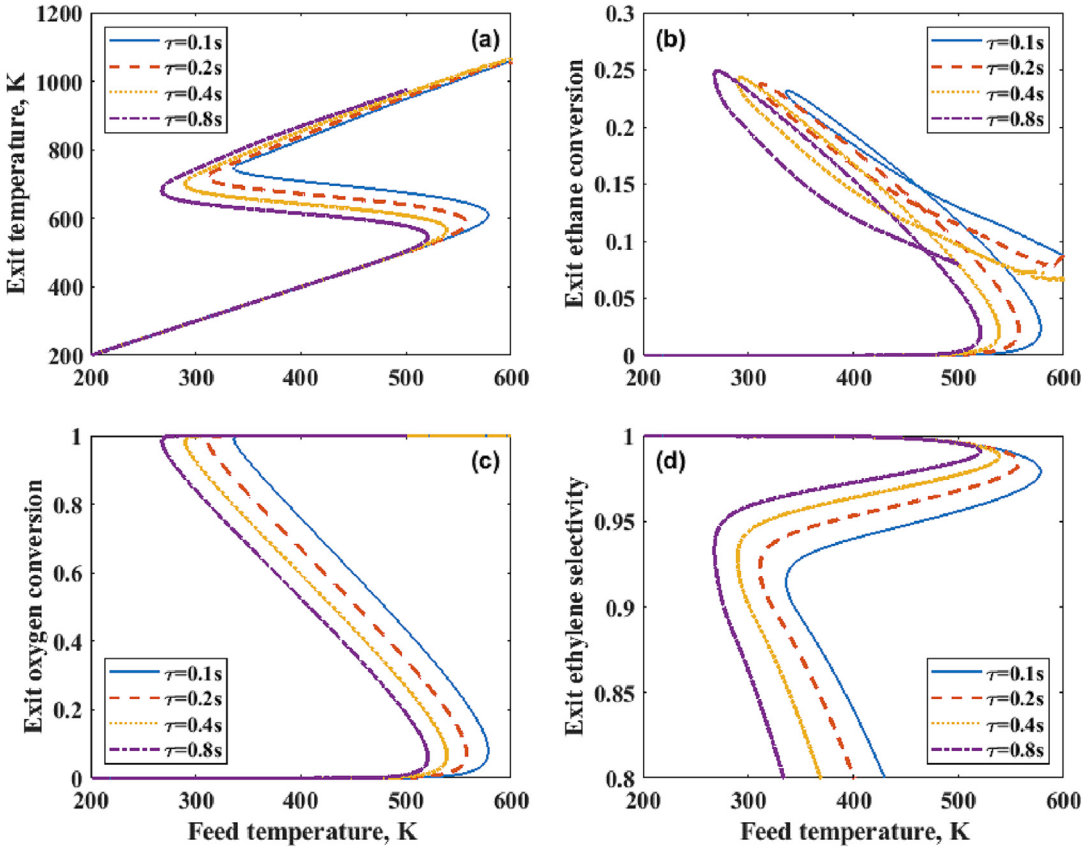

Fig. 4. Computed bifurcation diagrams of exit (a) temperature, (b) ethane conversion, (c) oxygen conversion, and (d) ethylene selectivity versus feed temperature at different space times for the finite heat dispersion model. Reaction conditions: C_2H_6 : O_2=6, bed length = 4 mm.

proportional to space time. Increasing the operating pressure at the same mass velocity could decrease the linear velocity and increase space time. The reaction rate is normally proportional to pressure for first order kinetics but the productivity does not change under this circumstance. On the other hand, operating at high pressures at a fixed linear velocity could increase the mass velocity, leading to higher productivity. We demonstrate these two cases separately in this section.

4.1. Fixed linear velocity

Fig. 7 shows the impact of total pressure on exit temperature, ethane conversion, and ethylene selectivity with fixed linear velocity and constant C_2H_6:O_2 feed ratio of 6, space time of 0.2 s, and bed length of 4 mm. Increasing the total pressure from 1 to 10 bar leaves the ignition temperature unaltered, while the extinction point moves to lower feed temperatures when the pressure increases from 1 to 5 bar and remains nearly the same for further pressure increases from 5 to 10 bar. Two reasons can help explain these results. For the specific ODHE kinetics under consideration, side reactions exhibit a higher pressure dependency than the desired dehydrogenation reaction, as can be seen from the rate expressions in Table S1. Side reactions therefore play a more important role and generate more heat as the total pressure increases, leading to a larger region of multiplicity from 1 to 5 bar. The effective mass and thermal dispersion coefficients can be calculated using the following equations:

$$D_{eff,j} = D_{m,j} + 0.5 < u > d_p,\ j = 1, 2, \cdots N, \tag{19}$$

$$\alpha_{eff} = \alpha_{s,eff} + 0.5 < u > d_p, \tag{20}$$

where $D_{m,j}$ is the mass diffusivity of species j, $< u >$ is the average gas velocity, d_p is the particle size, and $\alpha_{s,eff}$ is the catalyst bed thermal diffusivity. When the particle size is smaller than 1 mm and the space time is around 0.2 s, the second term in equations (19) and (20) is essentially one to two orders of magnitude smaller than the first term. Thus, heat dispersion decreases as total operating pressure increases since heat diffusivity is almost inverse first order in total pressure. This can help explain the fact that the region of multiplicity stays almost the same even though a larger amount of heat is generated as the total pressure increases from 5 to 10 bar. It can also be observed that ethane conversion and ethylene selectivity decrease with increasing total pressure. As explained above, side reactions are more dominant at higher operating pressures and therefore decrease ethane conversion and ethylene selectivity. Although higher total pressure tends to lower ethane conversion and ethylene selectivity, we note here that the ODHE process can still have about 20% per pass ethane conversion and 88% ethylene selectivity at a space time of 0.2 s at 5 bar.

In Fig. 8, we explore the effect of total pressure for different reactor lengths with the same space time of 0.2 s and a C_2H_6:O_2 feed ratio of 6. The feed temperature at the extinction point for an 8 mm bed is higher than that for a 4 mm bed, indicating that longer beds have weaker thermal backmixing. Therefore, the exit temperature at the extinction point calculated as the sum of the feed temperature and the adiabatic temperature rise is also higher for the 8 mm bed, suggesting lower exit ethylene selectivity as shown in Fig. 8**b and 8c**. It is also interesting to note that we observe multiple ignition and extinction points for the 8 mm bed at 5 bar as shown in Fig. 9. For an 8 mm bed, the reactor is first ignited at around T_f = 500 K and then passes the extinction point at around T_f = 300 K. After crossing the first extinction point, the

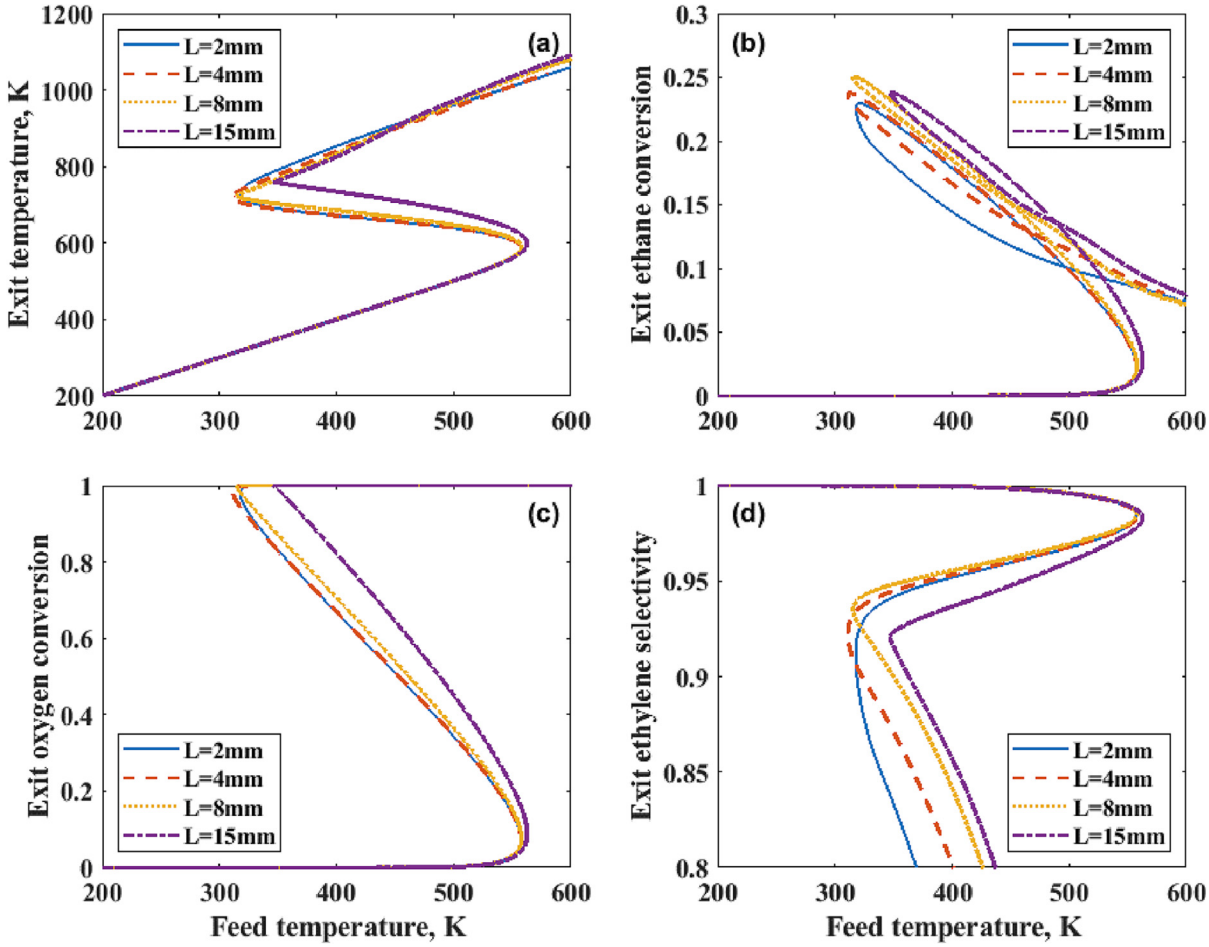

Fig. 5. Computed bifurcation diagrams of exit (a) temperature, (b) ethane conversion, (c) oxygen conversion, and (d) ethylene selectivity versus feed temperature with different bed lengths for the finite heat dispersion model. Reaction conditions: $C_2H_6 : O_2$=6, τ=0.2 s.

reactor can again be ignited at around T_f = 325 K and cross the second extinction point at around T_f = 300 K. A large amount of ethylene is produced on the first ignition branch at high operating pressures. Examination of the exit product composition shows that the second ignition and quenching behavior is caused by ethylene oxidation because the activation energies of the ethylene oxidation reactions (steps 4 and 5) are higher than that of the desired dehydrogenation reaction, but much lower than those for the deep oxidation reactions (steps 2 and 3). In contrast with our previous conclusion from Section 3.4, we note here that shallow beds are preferred so as to avoid the shrinking of regions of multiplicity and to ensure elimination of the second ignition and extinction behavior.

4.2. Fixed mass velocity

Unlike the case where total pressure is increased at a fixed linear velocity, when the mass velocity is instead kept constant, space times are proportional to the total pressure, resulting in no significant changes in productivity. Fig. 10 compares the impact of fixed linear velocity and fixed mass velocity on feed temperature, exit temperature, and exit ethylene selectivity at the extinction point as a function of total pressure for a constant C_2H_6:O_2 feed ratio of 6 and a bed length of 4 mm. It is found that the feed temperature at the extinction point decreases more significantly with increasing total pressure for the case of fixed mass velocity. As discussed in Section 4.1, the mass and thermal diffusivity exhibit nearly inverse first order dependence in total pressure. Although mass and thermal diffusivity decrease linearly with total pressure, higher space times at higher total pressures can still move the extinction point to lower feed temperatures. Exit temperatures at the extinction point at fixed mass velocity subsequently become lower compared to the case where linear velocity is held constant, resulting in an increment of ethylene selectivity at the extinction point as shown in Fig. 10**b and 10c**. But higher total pressures with fixed mass velocity (i.e. higher space time) could reduce feed temperature below the ambient temperature. For example, ensuring that the feed temperature is higher than 200 K constrains the operating pressure for the fixed mass velocity case to about 5 bar. Detailed bifurcation diagrams for the fixed mass velocity case are illustrated in Section S6 of the Supporting Information.

In order to have a better understanding of pressure effects in terms of fixed linear velocity and fixed mass velocity, we took P = 1 bar, τ=0.2 s as the base case and increased the pressure and space time while keeping either the linear velocity or mass velocity constant as shown in the Fig. 11. Other parameters like the C_2H_6:O_2 feed ratio and bed length were kept constant. As discussed above, the mass and thermal diffusivity decrease linearly with total pressure. Fixing the linear velocity leads to mass and heat Peclet numbers for case 2 being about 5 times higher than those for case 1, indicating weaker mass and heat dispersion. When fixing the mass velocity, the mass and heat Peclet numbers for case 3 are nearly identical to those for case 1. Side reactions are more dominant at higher operating pressures, leading to higher adiabatic temperature rise values. Although case 2 and case 3 carry the same or higher heat and mass Peclet numbers compared to case 1, the

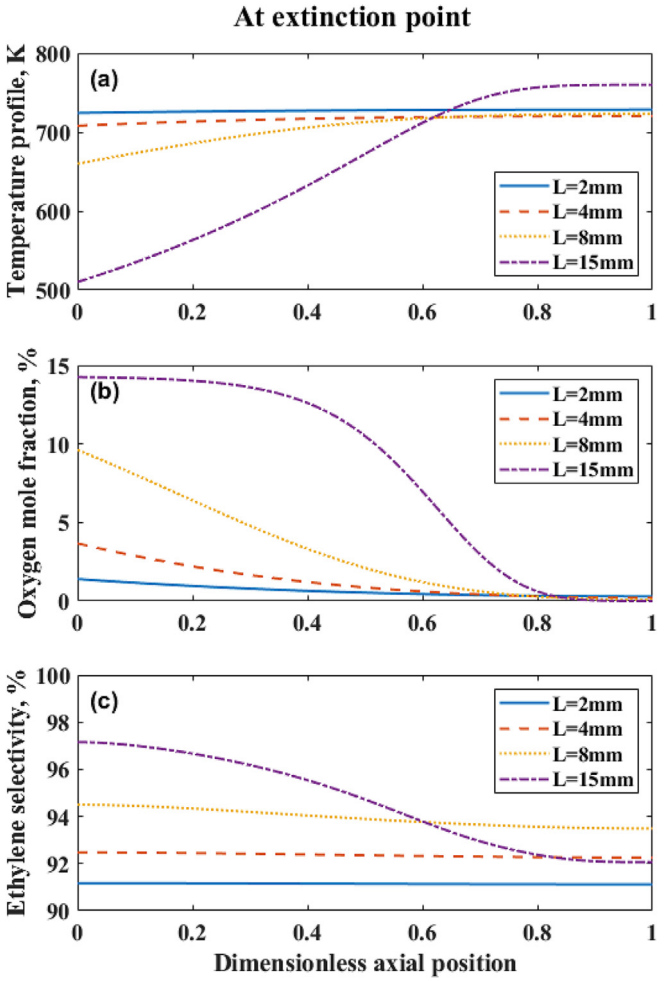

Fig. 6. Computed profiles of (a) temperature, (b) oxygen mole fraction, and (c) ethylene selectivity at the extinction point for different reactor lengths. Reaction conditions: C_2H_6 : O_2=6, τ=0.2 s.

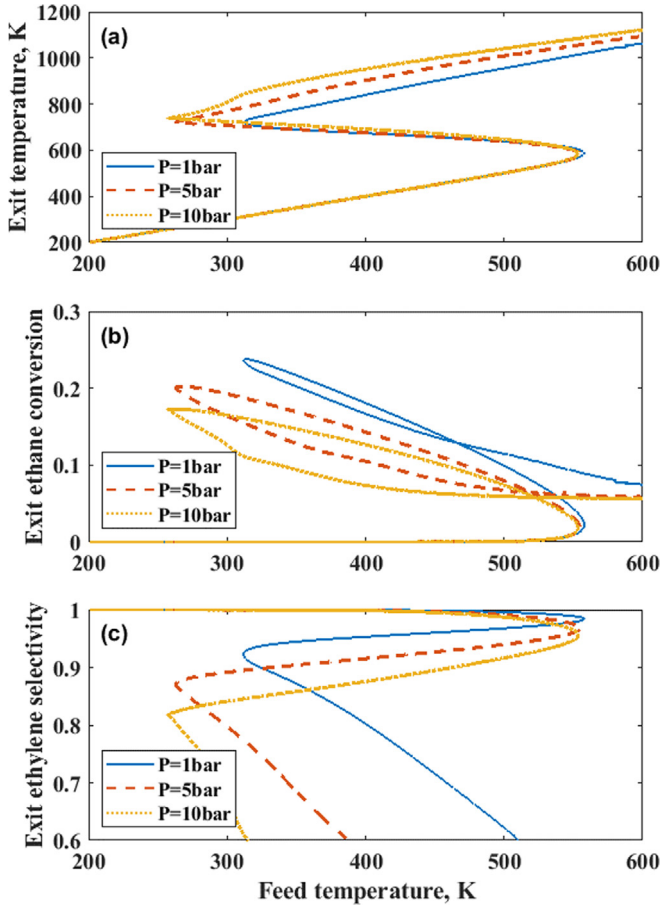

Fig. 7. Computed exit (a) temperature, (b) ethane conversion, and (c) ethylene selectivity versus feed temperature at different operating pressures with a fixed linear velocity. Reaction conditions: C_2H_6 : O_2=6, τ=0.2 s, bed length is 4 mm.

extinction point is found to occur at a lower feed temperature for case 2 and case 3 due to the higher adiabatic temperature rise observed at higher operating pressures as shown in Fig. 11**a**. Comparing bifurcation diagrams for cases 2 and 3, it can be observed that both the extinction and ignition points for case 3 move to lower feed temperatures because mass and heat Peclet numbers for case 2 are 5 times higher than those for case 3. This helps explain the observation that the exit temperature for case 3 at the extinction point is lower than that for case 2, leading to higher ethane conversions and ethylene selectivity as shown in Fig. 11**b and c**. Despite the fact that case 3 has higher conversions and selectivity, case 2 appears to lead to a much higher productivity than case 3 due to a higher mass velocity. Finally, and crucially in the context of commercial operation, we emphasize the fact that the ODHE process can be operated autothermally at 5 bar with close-to-ambient temperature feeds to achieve about 20% per pass ethane conversion and 87% ethylene selectivity.

4.3. Comparison of multi-tubular and autothermal ODHE reactor configurations

Traditional multi-tubular reactor designs have been extensively discussed in the open literature. In this work, we use a global kinetic model to compare under similar reaction conditions the performance of multi-tubular and autothermal reactors. Detailed calculations for multi-tubular reactor design can be found in section S5 of the Supplementary Information. Figure S3 shows computed temperature, conversion, and ethylene selectivity profiles along the multi-tubular reactor. A C_2H_6:O_2 feed ratio of 6 was chosen to constrain the adiabatic temperature rise. Typical characteristic reaction time for the ODHE process over $MoVTeNbO_x$ catalysts was around 1 s at 593 K. Based on the hot spot criterion (Sun et al., 2019), a space time of 3 s was used to remove most of the heat generated in the reactor. These results clearly show that operating at large space times and high C_2H_6:O_2 feed ratios can render ODHE operation at atmospheric pressure using multi-tubular reactors practicable.

Table 2 compares reactor specifications for multi-tubular and autothermal ODHE reactors at a 1000 kT (kilo tons) ethylene production scale. 1 in. (2.54 cm) tubes were used to minimize radial thermal gradients and to increase the heat exchange area per unit reaction volume. A 3 m long tube was chosen for efficient heat removal and for maintaining a reasonable pressure drop. The 1000 kTA (kilo tons per annum) ethylene production capacity is met using 15–20 multi-tubular reactors consisting of 20,000 identical tubes. As for the autothermal reactor, the production capacity can be met using a bed length of only 5 cm with the $MoVTeNbO_x$ catalyst coated or filled in the channels of a high thermal conductivity SiC substrate to increase thermal dispersion. 10–12 identical autothermal reactors are used in the plant, and a reactor diameter of only about 4.3 m can be used to minimize temperature patterns (Shah et al., 2022). We find that the autothermal reactor can be operated at a pressure of 5 bar and a space time of 0.2 s, resulting

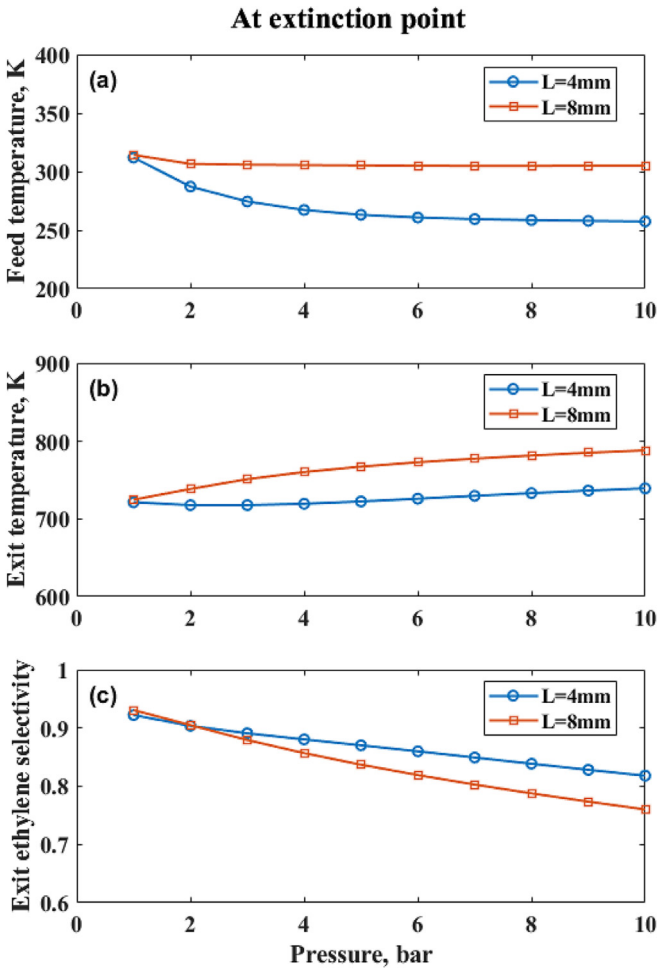

Fig. 8. Calculated (a) feed temperature, (b) exit temperature, and (c) exit ethylene selectivity at extinction point versus total pressure for different bed lengths with fixed linear velocity. Reaction conditions: C_2H_6 : O_2=6, τ=0.2 s.

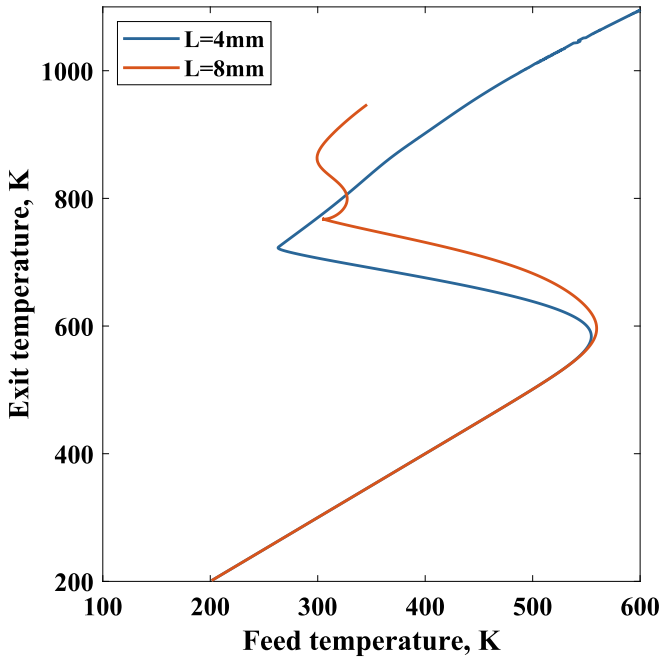

Fig. 9. Bifurcation diagram of exit temperature versus feed temperature for different bed lengths for high operating pressures. Reaction conditions: C_2H_6 : O_2=6, τ=0.2 s, P_{total} = 5 bar.

in an almost 75 times higher productivity than the multi-tubular reactor operating at a pressure of 1.2 bar and a space time of 3 s. The autothermal reactor does however have a slightly lower ethane conversion and ethylene selectivity owing to the higher operating temperature and pressure compared to the multi-tubular reactor. Based on our calculations, the total volume of the autothermal reactor configuration can be as much as a factor of 50 lower than that of the multi-tubular reactor, translating to lower footprints and capital expenses.

4.4. Comparison of high pressure ODHE and steam cracking

At present, ethylene is exclusively produced by steam cracking of liquid feedstock such as naphtha and gas oil or light alkanes such as ethane and propane. The steam cracking process is highly energy intensive, accounts for 8% of the energy usage in the chemical industry, and results in 180–200 million tons of CO_2 emissions annually (Ren et al., 2006). The oxidative dehydrogenation of ethane is considered as an alternative to the traditional steam cracking process. We therefore compare here the performance of an ethane steam cracker and the ODHE process implemented autothermally over a $MoVTeNbO_x$ catalyst. Fig. 12 shows the computed bifurcation diagram for exit temperature, exit ethane conversion, and exit product selectivity as a function of feed temperature calculated using the finite heat dispersion model. A C_2H_6:O_2 molar feed ratio of 4 was chosen to increase ethane conversion while avoiding a high value of adiabatic temperature rise, a space time of 0.3 s was chosen to avoid an unreasonably low feed temperature, and an operating pressure of 5 bar was chosen to achieve high productivity. A shallow pancake-like reactor (4 mm) was chosen to avoid multiple ignition and extinction behavior as discussed in Section 4.1. In the case of an ethane cracker, steam is co-fed with ethane to supply heat for driving the endothermic cracking reaction and to reduce the partial pressure of the hydrocarbon (Wittcoff et al., 2012). The typical steam to ethane mass ratio used is 0.35–0.45 kg/kg (Geem et al., 2004; Gujarathi et al., 2009), which translates to about 40% molar dilution. Analogously, the non-reactive nature of methane over the $MoVTeNbO_x$ catalyst allows us to apply 40% methane dilution in the autothermal reactor design. With all of these reaction conditions selected, the extinction point occurs at T_{in} = 250 K and T_{exit} = 705 K, as shown in Fig. 12**a**. The autothermal reactor configuration therefore makes it possible to achieve about 32% ethane conversion and 88% ethylene selectivity at 5 bar for ODHE.

Table 3 presents a comparison of reaction conditions and catalytic performance for an ethane cracker and the ODHE process. Typical temperatures for ethane crackers range from 750 to 850 °C, much higher than the operating temperature of the ODHE process which ranges between 350 and 450 °C. Further, the ODHE process can be operated at a pressure of 5 bar and a space time of 0.3 s, thereby achieving a twofold higher productivity compared to the ethane cracking process operated at a pressure of 1–1.2 bar and a space time of 0.1–0.4 s. We also note that the ODHE process can achieve about 32% ethane conversion and 88% ethylene selectivity when using an autothermal reactor, similar to the 50% ethane conversion and 80% ethylene selectivity typically achieved through ethane cracking. Not only is ethane cracking highly expensive also carbon-intensive owing to the fact that the endothermic nature of the process results in a large amount of carbon dioxide production from fuel combustion in the pyrolysis section (Mynko et al., 2022). In contrast with steam cracking, autothermally operated ODHE circumvents the need for external heat supply in the reactor and only generates approximately 0.77 kg CO_2/ kg ethylene due to the

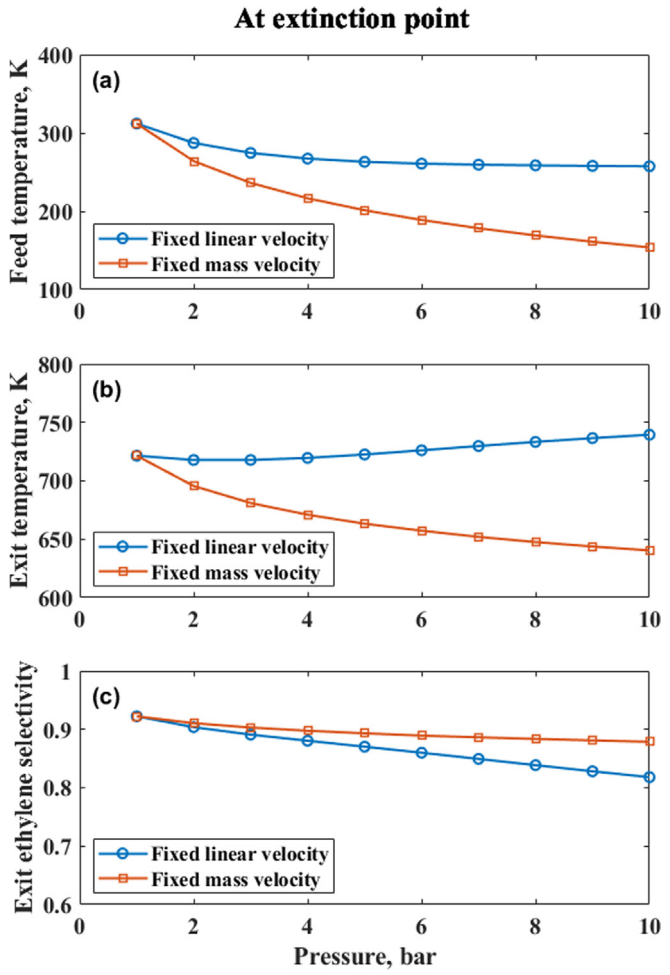

Fig. 10. Comparison of impact of fixed linear velocity and fixed mass velocity on (a) feed temperature, (b) exit temperature, and (c) exit ethylene selectivity at the extinction point with different total pressure when using the finite heat dispersion model. Reaction conditions: C_2H_6 : O_2=6, bed length is 4 mm.

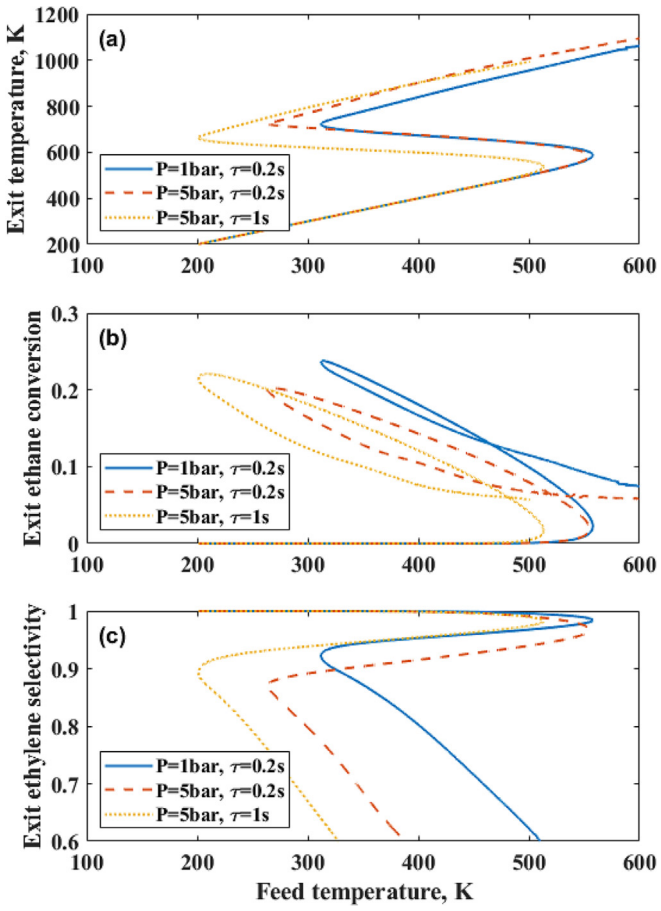

Fig. 11. Computed exit (a) temperature, (b) ethane conversion, and (c) ethylene selectivity versus feed temperature for three different cases. Case 1: P = 1 bar, τ=0.2 s, Case 2: P = 5 bar, τ=0.2 s, Case 3: P = 5 bar, τ=1.0 s. Reaction conditions: C_2H_6 : O_2=6, τ=0.2 s, bed length is 4 mm.

exceptionally high selectivity of the $MoVTeNbO_x$ catalyst, a carbon footprint that is 20% smaller than the 1.0 kg CO_2/kg ethylene produced when using the steam cracking process. More importantly, the CO_2 generated in the high pressure autothermal operation can be more easily captured and segregated.

5. Summary and discussion

The main contribution of this work is the detailed analysis of ignition and extinction behavior of an ODHE reactor and an illustration of the feasibility of autothermal operation based on a previously developed global kinetic model over a $MoVTeNbO_x$ catalyst. A second contribution is the demonstration by calculation that it is possible to operate the ODHE process at higher pressures. A third contribution is the comparison of the performance of an ODHE process implemented in an autothermal reactor to that of conventional steam cracking. We have shown that it is possible to operate ODHE autothermally using a thin bed (less than 10 mm) in the pseudo-homogeneous limit at a space time of 0.2 s and a C_2H_6:O_2 feed ratio of 6 at high pressures (5 bar). This leads to an ethane conversion of about 20–30% and an ethylene selectivity of about 85–95% depending on the operating temperature ranging between 650 and 750 K. The feed ratio of C_2H_6:O_2 is selected as 6 because higher feed ratios lead to lower ethane conversion and lower feed ratios lead to higher adiabatic temperature rise values, thereby lowering ethylene selectivity. The autothermal reactor design presented here is also sensitive to space time. We choose 0.2 s as the space time to make the extinction point close to ambient temperature while also simultaneously maintaining high productivity. Based on the kinetic model applied to the M1 phase catalyst, we can tune the bed length to change the temperature and oxygen concentration profiles along the catalyst bed such that there exists an optimum bed length of 8 mm to maximize ethane conversion and ethylene selectivity. We also investigated the effect of pressure on ignition and extinction behavior for cases where linear velocity and mass velocity were kept fixed. In the case of fixed linear velocity, although increasing the pressure expands

Table 2
Overview of multi-tubular and autothermal reactor operating conditions for a 1000 kTA ethylene production scale.

Multi-tubular reactor		Autothermal reactor	
Parameters	Value	Parameters	Value
Tube diameter	1 in.	Reactor diameter	4.3 *m*
Number of tubes	20,000	Reactor length	5 cm
Tube length	3 *m*	Number of reactors	10–12
Space time	3.0 s	Space time	0.2 s
Number of reactors	15–20	Temperature	683–703 K
Temperature	583–593 K	Pressure	5 bar
Pressure	1.2 bar	Ethane conversion	20–23 %
Ethane conversion	25–28%	Ethylene selectivity	86–90%
Ethylene selectivity	95–97%		

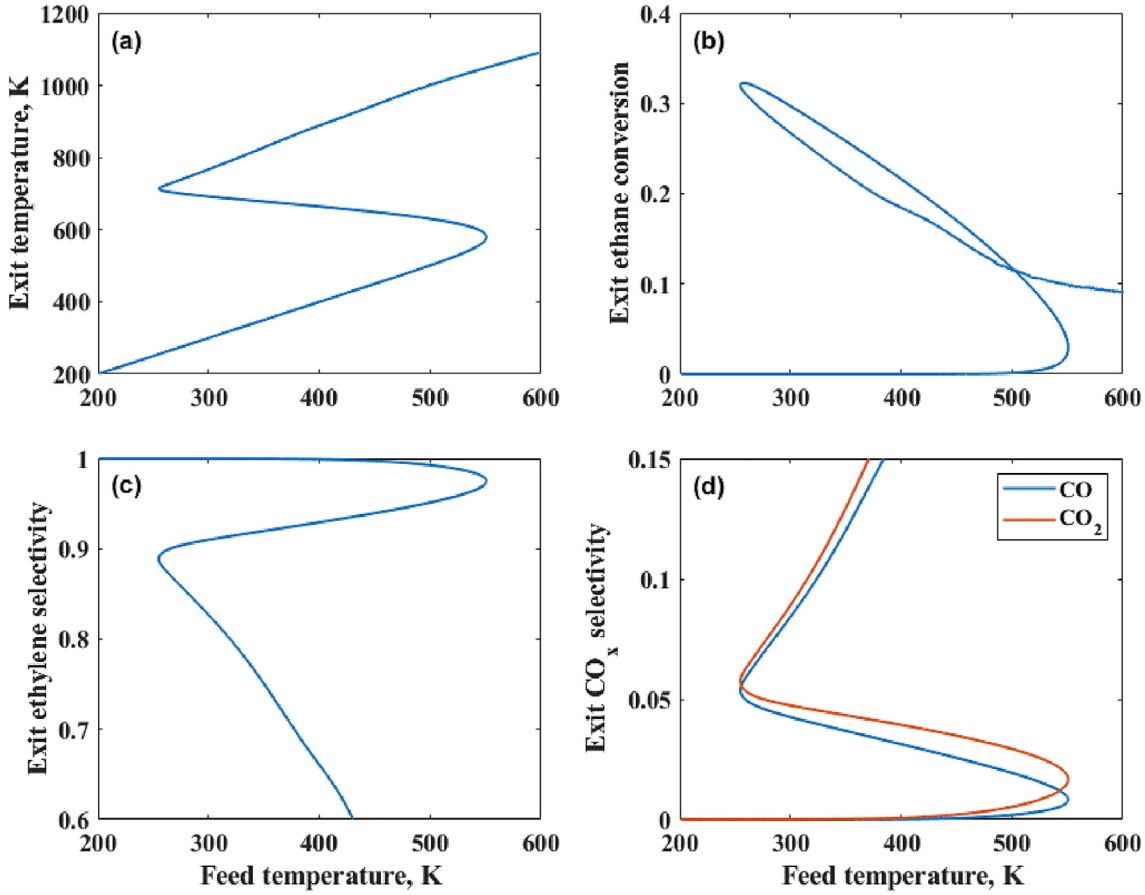

Fig. 12. Computed exit (a) temperature, (b) ethane conversion, (c) ethylene selectivity, and (d) CO_x selectivity versus feed temperature calculated using the finite heat dispersion model. Reaction conditions: C_2H_6 : O_2=4, τ=0.3 s, P_{total} = 5 bar, bed length = 4 mm, 40% methane dilution.

Table 3
Comparison of ethane cracking and ODHE processes in an autothermal reactor.

Conditions	Ethane Cracker	ODHE
Temperature, K	1000–1200 (Matar and Hatch, 2001)	620–720
Pressure, bar	1–1.2 (Matar and Hatch, 2001)	5
Space time, s	~0.1–0.4 (Ranjan et al., 2012; Wittcoff et al., 2012)	0.3
Ethane conversion, %	~50 (Sabbe et al., 2011)	32
Ethylene selectivity, %	~80 (Sabbe et al., 2011)	88
Dilution, %	40 (steam) (Geem et al., 2004)	40 (methane)
CO_2 emission, kg CO_2/ kg C_2H_4	~1.0 (Ren et al., 2006)	~0.77

the region of multiplicity, the ethane conversion and ethylene selectivity both drop because side reactions become more dominant at higher pressures. Furthermore, thinner beds favor higher ethane conversion and ethylene selectivity for high pressure operation and can avoid the existence of multiple ignition and extinction behavior. As for the case of fixed linear mass velocity, higher pressures can enlarge the region of multiplicity while still maintaining similar ethane conversion and ethylene selectivity. This is because the feed temperature at the extinction point is much lower than ambient temperature at high pressure and therefore the operating temperature is also lower. However, it is not practical to feed reactants below 200 K. Besides, we compared the performance of multi-tubular and autothermal reactors for the ODHE, and found that autothermal reactors can be 50 times smaller than multi-tubular ones with similar ethane conversion and ethylene selectivity. Lastly, the ODHE process can be operated at higher pressures (5 bar) and still enable 32% ethane conversion and 88% ethylene selectivity, similar to the performance noted in the ethane cracking process. In contrast with the autothermal reactor, ethane cracking can be only operated at lower pressures (1–1.2 bar) at a space time of 0.1–0.4 s, thereby resulting in lower productivity. Additionally, the ODHE process does not need any external heat supply from burning fuel and is thus more economically and environmentally viable.

We now discuss some limitations and possible extensions of the results presented here. For example, we only consider the pseudo-homogeneous finite heat dispersion model by assuming that the particle size is below 1 mm, which may result in a high pressure drop along the length of the bed. A detailed two-phase finite axial and radial heat dispersion model may be used in future work to investigate ignition and extinction behavior of the autothermal reactor. In addition, in this work we ignored the variation of the physical properties as well as any instability problems caused by coupling between energy and momentum balances (Agrawal et al., 2007). Therefore, extension of these results to 3D models will be of interest in future work.

Author Statement:

Jiakang Chen.: Model formulation and computations; writing original draft,

Zhe Sun: Help with computations, revisions of draft.

Praveen Bollini: Conceptualization, Methodology, revisions of the draft and research supervision.

Vemuri Balakotaiah: Conceptualization, Methodology, revisions of the draft and research supervision.

Data availability

Data will be made available on request.

Declaration of Competing Interest

The authors declare that they have no known competing financial interests or personal relationships that could have appeared to influence the work reported in this paper.

Acknowledgements

The authors acknowledge funding from the National Science Foundation (Grant # CBET-2133174).

Appendix A. Supplementary material

Supplementary data to this article can be found online at https://doi.org/10.1016/j.ces.2023.118649.

References

Abdelbaki, Y., de Arriba, A., Solsona, B., Delgado, D., García-González, E., Issaadi, R., López Nieto, J.M., 2021. The nickel-support interaction as determining factor of the selectivity to ethylene in the oxidative dehydrogenation of ethane over nickel oxide/alumina catalysts. Appl. Catal. A 623, 1–12. https://doi.org/10.1016/j.apcata.2021.118242.

Agrawal, R., West, D.H., Balakotaiah, V., 2007. Modeling and analysis of local hot spot formation in down-flow adiabatic packed-bed reactors. Chem. Eng. Sci. 62, 4926–4943. https://doi.org/10.1016/j.ces.2006.11.057.

Amghizar, I., Vandewalle, L.A., Van Geem, K.M., Marin, G.B., 2017. New Trends in Olefin Production. Engineering 3, 171–178. https://doi.org/10.1016/J.ENG.2017.02.006.

Annamalai, L., Liu, Y., Ezenwa, S., Dang, Y., Suib, S.L., Deshlahra, P., 2018. Influence of tight confinement on selective oxidative dehydrogenation of ethane on MoVTeNb mixed oxides. ACS Catal. 8, 7051–7067. https://doi.org/10.1021/acscatal.8b01586.

Balakotaiah, V., Sun, Z., Gu, T., West, D.H., 2021. Scaling relations for autothermal operation of catalytic reactors. Ind. Eng. Chem. Res. 60, 6565–6582. https://doi.org/10.1021/acs.iecr.0c05594.

Balakotaiah, V., Sun, Z., West, D.H., 2019. Autothermal reactor design for catalytic partial oxidations. Chem. Eng. J. 374, 1403–1419. https://doi.org/10.1016/j.cej.2019.05.155.

Bilgen, S., Sarıkaya, İ., 2016. New horizon in energy: shale gas. J. Nat. Gas Sci. Eng. 35, 637–645. https://doi.org/10.1016/j.jngse.2016.09.014.

Botella, P., García-González, E., Dejoz, A., López Nieto, J.M., Vázquez, M.I., González-Calbet, J., 2004. Selective oxidative dehydrogenation of ethane on MoVTeNbO mixed metal oxide catalysts. J. Catal. 225, 428–438. https://doi.org/10.1016/j.jcat.2004.04.024.

Cavani, F., Ballarini, N., Cericola, A., 2007. Oxidative dehydrogenation of ethane and propane: how far from commercial implementation? Catal Today 127, 113–131. https://doi.org/10.1016/j.cattod.2007.05.009.

Che-Galicia, G., Quintana-Solórzano, R., Ruiz-Martínez, R.S., Valente, J.S., Castillo-Araiza, C.O., 2014. Kinetic modeling of the oxidative dehydrogenation of ethane to ethylene over a MoVTeNbO catalytic system. Chem. Eng. J. 252, 75–88. https://doi.org/10.1016/j.cej.2014.04.042.

Che-Galicia, G., Ruiz-Martínez, R.S., López-Isunza, F., Castillo-Araiza, C.O., 2015. Modeling of oxidative dehydrogenation of ethane to ethylene on a MoVTeNbO/TiO_2 catalyst in an industrial-scale packed bed catalytic reactor. Chem. Eng. J. 280, 682–694. https://doi.org/10.1016/j.cej.2015.05.128.

Chen, J., Bollini, P., Balakotaiah, V., 2021. Oxidative dehydrogenation of ethane over mixed metal oxide catalysts: Autothermal or cooled tubular reactor design? AIChE J 67, 1–13. https://doi.org/10.1002/aic.17168.

Chen, J., Sun, Z., Balakotaiah, V., Bollini, P., 2022. A global kinetic model for the oxidative dehydrogenation of ethane over mixed metal oxide catalysts at supra-ambient pressures. Chem. Eng. J. 445,. https://doi.org/10.1016/j.cej.2022.136605 136605.

Chen, L., Pannala, S., Broekhuis, R., Gautam, P., Gu, T., West, D., Balakotaiah, V., 2020. Three-dimensional CFD simulation of pattern formation in a shallow packed-bed reactor for oxidative coupling of methane. Chem. Eng. J. 400,. https://doi.org/10.1016/j.cej.2020.125979 125979.

Chu, B., Truter, L., Nijhuis, T.A., Cheng, Y., 2015. Performance of phase-pure M1 $MoVNbTeO_x$ catalysts by hydrothermal synthesis with different post-treatments for the oxidative dehydrogenation of ethane. Appl. Catal. A 498, 99–106. https://doi.org/10.1016/j.apcata.2015.03.039.

Fazlinezhad, A., Naeimi, A., Yasari, E., 2019. Theoretical investigation of ethane oxidative dehydrogenation over MoVTeNbO catalyst in fixed-bed reactors with intermediate water removal. Chem. Eng. Res. Des. 146, 427–435. https://doi.org/10.1016/j.cherd.2019.04.028.

Fuller, E.N., 1965. A comparison of methods for predicting gaseous diffusion coefficients. J. Chromatogr. Sci. 3, 222–227. https://doi.org/10.1093/chromsci/3.7.222.

Gaffney, A.M., Duprez, N.V., Louthan, K.J., Borders, B., Gasque, J., Siegfried, A., Stanford, T.G., Roberts, K.L., Alcheikhhamdona, Y., Hoorfar, M., Chen, B., Majumdar, S., Murnen, H., 2021a. Ethylene production using oxidative dehydrogenation: effects of membrane-based separation technology on process safety & economics. Catal. Today 371, 11–28. https://doi.org/10.1016/j.cattod.2020.07.063.

Gaffney, A.M., Mason, O.M., 2017. Ethylene production via oxidative dehydrogenation of ethane using M1 catalyst. Catal. Today 285, 159–165. https://doi.org/10.1016/j.cattod.2017.01.020.

Gaffney, A.M., Sims, J.W., Martin, V.J., Duprez, N.V., Louthan, K.J., Roberts, K.L., 2021b. Evaluation and analysis of ethylene production using oxidative dehydrogenation. Catal. Today 369, 203–209. https://doi.org/10.1016/j.cattod.2020.06.017.

Geem, K.M.V., Heynderickx, G.J., Marin, G.B., 2004. Steam Cracking 50, 173–183. https://doi.org/10.1002/aic.10016.

Ghani, R., Iranshahi, D., 2019. Comparison of co-current and counter-current flow in a bifunctional reactor containing ammonia synthesis and 2-butanol dehydrogenation to MEK. Int. J. Hydrogen Energy 44, 2905–2917. https://doi.org/10.1016/j.ijhydene.2018.11.028.

Gujarathi, A.M., Patle, D.S., Agarwal, P., Karemore, A.L., Babu, B.V., 2009. Simulation and analysis of ethane cracking process. Chem. Eng. 031, 2–8.

Haribal, V.P., Neal, L.M., Li, F., 2017. Oxidative dehydrogenation of ethane under a cyclic redox scheme – process simulations and analysis. Energy 119, 1024–1035. https://doi.org/10.1016/j.energy.2016.11.039.

Heracleous, E., Lemonidou, A.A., 2006a. Ni-Nb-O mixed oxides as highly active and selective catalysts for ethene production via ethane oxidative dehydrogenation. Part II: Mechanistic aspects and kinetic modeling. J. Catal. 237, 175–189. https://doi.org/10.1016/j.jcat.2005.11.003.

Heracleous, E., Lemonidou, A.A., 2006b. Ni-Nb-O mixed oxides as highly active and selective catalysts for ethene production via ethane oxidative dehydrogenation. Part I: Characterization and catalytic performance. J. Catal. 237, 162–174. https://doi.org/10.1016/j.jcat.2005.11.002.

Kolen'ko, Y. V., Zhang, W., Naumann d'Alnoncourt, R., Girgsdies, F., Hansen, T.W., Wolfram, T., Schlögl, R., Trunschke, A., 2011. Synthesis of MoVTeNb oxide catalysts with tunable particle dimensions. ChemCatChem 3, 1597–1606. 10.1002/cctc.201100089.

López Nieto, J.M., Botella, P., Vázquez, M.I., Dejoz, A., 2002. The selective oxidative dehydrogenation of ethane over hydrothermally synthesised MoVTeNb catalysts. Chem. Commun. 4, 1906–1907. https://doi.org/10.1039/b204037a.

Luongo, G., Donat, F., Krödel, M., Cormos, C.C., Müller, C.R., 2021. Experimental data supported techno-economic assessment of the oxidative dehydrogenation of ethane through chemical looping with oxygen uncoupling. Renew. Sustain. Energy Rev. 149. https://doi.org/10.1016/j.rser.2021.111403.

Matar, S., Hatch, L.F., 2001. Chemistry of petrochemical processes. Elsevier.

Melzer, D., Mestl, G., Wanninger, K., Zhu, Y., Browning, N.D., Sanchez-Sanchez, M., Lercher, J.A., 2019. Design and synthesis of highly active MoVTeNb-oxides for ethane oxidative dehydrogenation. Nat. Commun. 10, 1–9. https://doi.org/10.1038/s41467-019-11940-0.

Mynko, O., Amghizar, I., Brown, D.J., Chen, L., Marin, G.B., de Alvarenga, R.F., Uslu, D. C., Dewulf, J., Van Geem, K.M., 2022. Reducing CO_2 emissions of existing ethylene plants: Evaluation of different revamp strategies to reduce global CO_2 emission by 100 million tonnes. J. Clean. Prod. 362. https://doi.org/10.1016/j.jclepro.2022.132127.

Nawaz, Z., 2016. Heterogeneous reactor modeling of an industrial multitubular packed-bed ethylene oxide reactor. Chem. Eng. Technol. 39, 1845–1857. https://doi.org/10.1002/ceat.201500603.

Nguyen, T.T., Aouine, M., Millet, J.M.M., 2012. Optimizing the efficiency of MoVTeNbO catalysts for ethane oxidative dehydrogenation to ethylene. Catal. Commun. 21, 22–26. https://doi.org/10.1016/j.catcom.2012.01.026.

Qian, S., Chen, Y., Yan, B., Cheng, Y., 2022. Plasma treated M1 $MoVNbTeO_x$–CeO_2 composite catalyst for improved performance of oxidative dehydrogenation of ethane. Green Energy Environ. 1–11. https://doi.org/10.1016/j.gee.2022.01.001.

Rahman, F., Loughlin, K.F., Al-Saleh, M.A., Saeed, M.R., Tukur, N.M., Hossain, M.M., Karim, K., Mamedov, A., 2010. Kinetics and mechanism of partial oxidation of ethane to ethylene and acetic acid over MoV type catalysts. Appl. Catal. A 375, 17–25. https://doi.org/10.1016/j.apcata.2009.11.026.

Ranjan, P., Kannan, P., Al Shoaibi, A., Srinivasakannan, C., 2012. Modeling of ethane thermal cracking kinetics in a pyrocracker. Chem. Eng. Technol. 35, 1093–1097. https://doi.org/10.1002/ceat.201100529.

Ren, T., Patel, M., Blok, K., 2006. Olefins from conventional and heavy feedstocks : Energy use in steam cracking and alternative processes 31, 425–451. 10.1016/j.energy.2005.04.001.

Rodríguez, M.L., Ardissone, D.E., López, E., Pedernera, M.N., Borio, D.O., 2011. Reactor designs for ethylene production via ethane oxidative dehydrogenation: comparison of performance. Ind. Eng. Chem. Res. 50, 2690–2697. https://doi.org/10.1021/ie100738q.

Sabbe, M.K., Geem, K.M.V., Reyniers, M.-F., Marin, G.B., 2011. First principle-based simulation of ethane steam cracking. AIChE J 57, 482–496. https://doi.org/10.1002/aic.12269.

Sanfiz, A.C., Hansen, T.W., Teschner, D., Schnörch, P., Girgsdies, F., Trunschke, A., Schlögl, R., Looi, M.H., Hamid, S.B.A., 2010. Dynamics of the MoVTeNb oxide M1 phase in propane oxidation. J. Phys. Chem. C 114, 1912–1921. https://doi.org/10.1021/jp909352u.

Sarsani, S., West, D., Liang, W., Balakotaiah, V., 2017. Autothermal oxidative coupling of methane with ambient feed temperature. Chem. Eng. J. 328, 484–496. https://doi.org/10.1016/j.cej.2017.07.002.

Shah, M., West, D., Balakotaiah, V., 2022. Bifurcation and stability analysis of temperature patterns in shallow-bed catalytic reactors. Chem. Eng. J. 446,. https://doi.org/10.1016/j.cej.2022.137146 137146.

Sun, Z., West, D.H., Balakotaiah, V., 2019. Bifurcation analysis of catalytic partial oxidations in laboratory-scale packed-bed reactors with heat exchange. Chem. Eng. J. 377, 1–17. https://doi.org/10.1016/j.cej.2018.08.151.

Sun, Z., West, D.H., Gautam, P., Balakotaiah, V., 2020. Scale-up analysis of autothermal operation of methane oxidative coupling with La_2O_3/CaO catalyst. AIChE J 66, 1–14. https://doi.org/10.1002/aic.16949.

Valente, J.S., Quintana-Solórzano, R., Armendáriz-Herrera, H., Barragán-Rodríguez, G., López-Nieto, J.M., 2014. Kinetic study of oxidative dehydrogenation of ethane over MoVTeNb mixed-oxide catalyst. Ind. Eng. Chem. Res. 53, 1775–1786. https://doi.org/10.1021/ie402447h.

Wittcoff, H., A., B., Reuben, G., Plotkin, effery S., 2012. Industrial organic chemicals, John Wiley. ed.